Talbot-Lau X-ray Deflectometer: Refraction-based HEDP imaging diagnostic

M. P. Valdivia,[1,a)] D. Stutman,[1] C. Stoeckl,[2] W. Theobald,[2] G. W. Collins IV,[3] V. Bouffetier,[4] M. Vescovi,[5] C. Mileham,[2] I. A. Begishev,[2] S. R. Klein,[6] R. Melean,[6] S. Muller,[7] J. Zou,[2] F. Veloso,[5] A. Casner,[8] F. N. Beg,[3] S. P. Regan[2]

[1] *Physics and Astronomy Department, Johns Hopkins University, Baltimore, Maryland 21218, USA*
[2] *Laboratory for Laser Energetics, University of Rochester, Rochester, New York 14623, USA*
[3] *Center for Energy Research, University of California San Diego, San Diego, California 92093, USA*
[4] *Université de Bordeaux-CNRS-CEA, Centre Lasers Intenses et Applications, UMR5107, F-33405 Talence, France*
[5] *Pontificia Universidad Catolica de Chile, Casilla 306, Santiago, Chile*
[6] *University of Michigan, Ann Arbor, Michigan 48109, USA*
[7] *General Atomics, Inertial Fusion Technology, San Diego, California 92921, USA*
[8] *CEA-CESTA, 15 avenue des Sablières, CS 60001, 33116 Le Barp CEDEX, France*

(Presented XXXXX; received XXXXX; accepted XXXXX; published online XXXXX)

Talbot-Lau x-ray interferometry has been implemented to map electron density gradients in HEDP experiments. X-ray (8 keV) backlighters have been evaluated for Talbot-Lau X-ray Deflectometry (TXD). Thin Cu foils, wires, and sphere targets have been irradiated by 10-150 J, 8-30 ps laser pulses, while two pulsed-power generators (~350 kA, 350 ns and ~200 kA, 150 ns) have driven Cu wire, hybrid, and laser-cut x-pinches. A plasma ablation front generated by the Omega EP laser was imaged, for the first time, through TXD for densities >10^{23} cm^{-3}. Backlighter optimization in combination with x-ray CCD, image plate, and x-ray film has been assessed in context of spatial resolution and interferometer contrast for accurate plasma characterization through TXD in the pulsed-power and high-intensity laser environments. Results obtained thus far demonstrate the potential of TXD as a powerful diagnostic for HEDP experiments.

I. INTRODUCTION

When probing weakly absorbing materials with 1-100 keV x-rays, refraction effects are dominant. For low-Z, the real part of the index of refraction $n = 1 - \delta + i\beta$ is much larger than the imaginary part (Fig. 1). Thus, x-ray phase contrast imaging can provide far better contrast than attenuation radiography techniques in High Energy Density (HED) plasma experiments within this energy range[1].

Talbot-Lau X-ray Deflectometry (TXD) is a refraction-based electron density gradient diagnostic for highly dense matter[2]. TXD implementations in the high-intensity laser and pulsed-power environments will be presented. Optimization of x-ray backlighter emission and spatial resolution will be discussed in context of detector and backlighter targets. Future developments of the TXD technique will be discussed.

II. TALBOT-LAU INTERFEROMETRY

Talbot-Lau (TL) interferometry is commonly used in synchrotron facilities or in conjunction with medical x-ray tubes for biological imaging or material science[3,4]. This phase-contrast imaging technique that can deliver electron density gradients information in plasmas by measuring x-ray refraction angles using the following equation:

$$\alpha(x) = \frac{\lambda^2 r_e}{2\pi} \frac{\partial}{\partial x} \int N_e\,(x,y)dy \qquad (1)$$

where α is angular refraction, λ probing beam wavelength, r_e electron radius, and N_e electron density.

[a)]Correspondence should be addressed: mvaldiv2@jhu.edu

A probing x-ray beam will be deviated due to the changes in index of refraction within a sample. Hence, highly dense objects can be diagnosed by measuring the x-ray refraction angle[2,5,6]. It should be noted that Talbot-Lau interferometry integrates along the direction of the probing beam, in similarity to standard x-ray imaging diagnostics. Hence TL interferometry measures line integrated electron density gradient information directly.

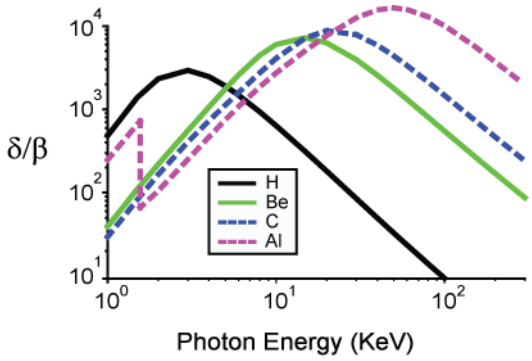

FIG. 1 H, Be, C, Al, and Au δ/β ratio for 1-100 keV probing beams.

TL interferometry uses micro-periodic gratings (source, phase, and analyzer) to measure small angular deviations of a beam transversing an object (Fig. 2). The source grating g_0 ensures x-ray coherence by generating an array of micro-sources[7–9]. TL interferometry works with incoherent and polychromatic x-ray sources such as those available in the high-intensity laser or the pulsed-power environments.

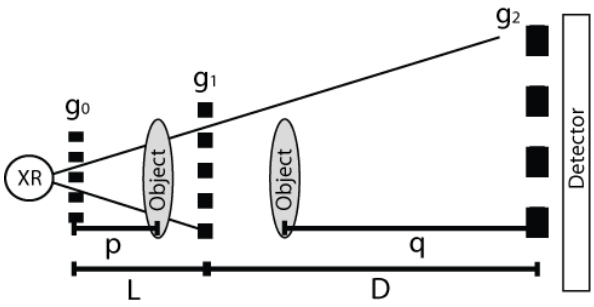

FIG. 2 Talbot-Lau interferometer configurations. Probed object can be located between g_0 and g_1 or g_1 and g_2.

Constructive image formation is achieved when $g_0 = g_2 (L/D)$ where g_i is the period of the grating and L, D are shown in Figure 2. The phase grating g_1 is typically a π-shift grating, splitting the beam into ±1 orders, set at the Talbot distance[10] $d_T = m\, g_1^2 / 8\, \lambda$, where m is the (odd) order of the interference pattern. Is important to note that each Talbot order has a specific interferometer contrast curve (Figure 3) so that larger orders have a narrower energy bandwidth due to a narrower contrast peak centered at the interferometer design energy. Considering Equation 1, when solving for electron density, a narrower energy bandwidth translates to a more accurate measurement. Additionally, Talbot orders translate to larger interferometer length. In a magnifying geometry, d_T scales with Talbot magnification $M_T = (D+L)/L$. The analyzer grating g_2 turns refraction angle changes into intensity changes at the detector plane.

III. TALBOT-LAU INTERFEROMETRY IN HEDP

Talbot-Lau interferometry was proposed recently as a HED plasma diagnostic[5,11]. By providing refraction-based images, TL imaging can characterize highly dense regions in plasmas by measuring electron density gradients through refraction angle detection. Post-processing can provide electron density maps with high spatial resolution. TL interferometry can identify regions of hydrodynamic instabilities, for example, not observable in conventional radiography due to lack of attenuation contrast[1].

Talbot-Lau X-ray Deflectometry (TXD)[6,12,13] has been developed, where the analyzer is rotated a small angle ($\Theta \approx \sin\Theta$), producing a Moire pattern with period $P_M = (g_2/2)\sin(\Theta/2)$. The refraction angle is given by $\alpha \approx W_{eff}\, F$, where W_{eff} is the effective angular resolution of the interferometer and F is the fringe shift. Effective angular resolution is given by[14]: (a) g_0/p when the object is located between g_0 and g_1 and *p* is the distance between the object and g_0 or (b) g_2/q when the object is located in between g_1 and g_2 and *q* is the distance between the object and g_2, as shown in Figure 2. The fringe shift is measured through Fourier techniques, separating phase-shift from attenuation, thus obtaining simultaneous information from a single Moire image[2].

The TL interferometers had periods of 2.4, 3.85, and 12 μm for g_0, g_1, and g_2, respectively (as described in Ref. 15) and were set in m = 1, 3, 5, and 7 with $M_T = 6$ for all configurations. Figure 3 shows the interferometer contrast curve along with 8 keV emission expected from Cu laser-target interactions and x-pinch discharges. Fringe contrast is a measure of the interferometer quality. In TXD, contrast is defined as the ratio between the intensity amplitude and the intensity mean of the signal. It is worth noting that energy bandwidth is proportional to 1/m, hence, larger Talbot orders increase the accuracy of electron density retrieval, as per Equation 1.

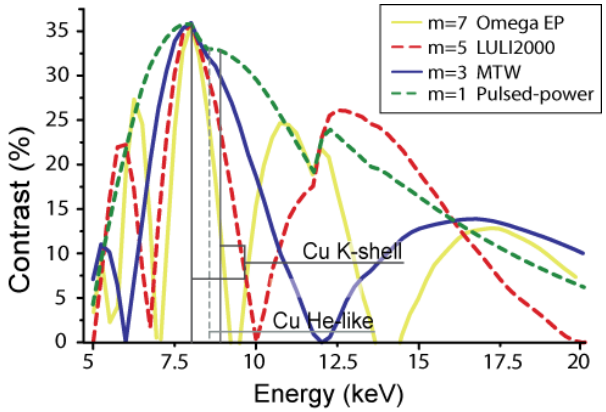

FIG. 3 Talbot-Lau m = 1, 3, 5, and 7 contrast curves for g_0 = 2.4 μm, g_1 = 3.85 μm, and g_2 = 12 μm. Cu emission also plotted.

IV. TXD FOR HIGH-INTENSITY LASER EXPERIMENTS

TXD has been benchmarked on MTW, LULI2000, and OMEGA EP lasers[15–17]. MTW experiments demonstrated grating survival and Moiré fringe formation irradiating thin Cu foils at 45° with $I \sim 5 \times 10^{16}$ W/cm^2 (<30 J, 8 ps). Electron density of a solid static object was retrieved with ~92% accuracy and spatial resolution of 50 μm was measured[15]. Moire images were recorded in LULI2000 experiments (2×10^{14} W/cm^2) with <60 J, 10 ps laser pulses. Image plates showed lower contrast than x-ray CCD images recorded on MTW, 7% compared to <25%, respectively[16]. Resolution of 24 μm was measured for 25 μm diameter wire Cu targets[18], motivating follow-up MTW experiments using wire and sphere Cu targets of 20 μm and 14-25 μm diameter, achieving <25 μm spatial resolution[16].

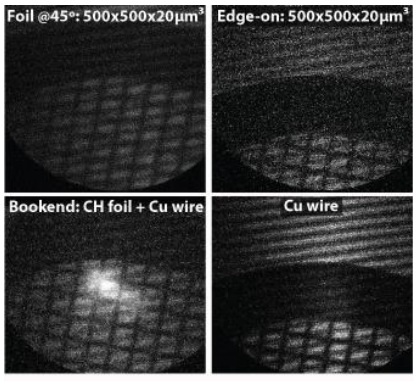

FIG. 4 MTW Moire images of Cu grids recorded with x-ray CCD. Spatial resolution for Cu foils (top) and wires (bottom) was measured at ~5-10 μm. Note that color scale and contrast have been modified.

In recent studies, "bookend" targets[19] composed of Cu wire wedged between two CH foils, were tested alongside

Cu wires, spheres, and edge-on planar foils. In these experiments, laser spot size was also changed for each target to optimize fringe contrast by varying laser intensity (I ~8-30 × 10^{15} W/cm^2). A future publication will address x-ray backlighter optimization through laser intensity and target type variation. Cu grid images (Fig. 4) were used to measure spatial resolution in the vertical and horizontal directions, that is, parallel and perpendicular to the grating bars, respectively. Spatial resolutions (at the object plane) of ~5-10 µm FWHM were measured for edge-on foils, wires, spheres, and bookend targets. Considering pixel size, the measurements were restricted to 3-5 µm which varied depending on detector binning and object magnification.

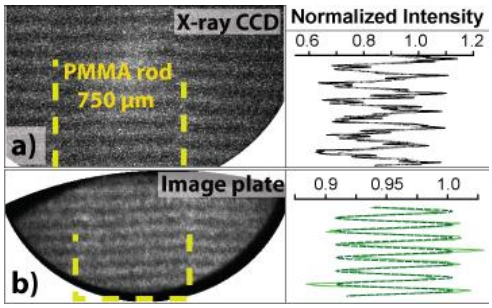

FIG. 5 MTW Moire images of a plastic PMMA rod of 750 µm diameter recorded with: a) X-ray CCD and b) Image plate. Normalized intensity profiles used to measure contrast are shown on the right. Moire image color contrast enhanced to better showcase fringe shift.

Fringe contrast loss was observed (<22 %) and caused by high-energy emission from wire, sphere, and bookend targets due to hot electron generation[17], which has been observed in experiments[20,21] with laser intensities >10^{18} W/cm^2. Lower fringe contrast of ~5% was measured with image plates (Fig. 5) as they have lower gain at <10 keV and higher gain at >20 keV, unlike x-ray CCD detectors.

A TXD diagnostic has been implemented on Omega EP. Laser pulses of 50-150 J, 10 ps (1-3 × 10^{17} W/cm^{-2}) were used to drive Cu foil, wire, and bookend targets[16]. To identify optimal target type, a HOPG spectrometer measured Cu K-shell emission and interferometer contrast was determined from Moire images. Spatial resolution of >60 µm was measured for Cu foils at 45º in the first Omega EP campaign (Fig. 6a)[17]. In a new Omega EP campaign, >10 µm spatial resolution was measured for Cu foil targets at normal laser incidence (Fig. 6b), that is, edge-on orientation with respect to TXD line-of-sight.

As in MTW experiments, improved spatial resolution for edge-on Cu foil backlighters targets was accompanied by additional high-energy emission. In 8 keV Talbot-Lau X-ray Deflectometry, x-ray emission outside the contrast curve (Fig. 3) will contribute to Moire image intensity base levels, thus diminishing contrast. On Omega EP, fringe contrast of 3-10% was measured for edge-on Cu foils, compared to 11-17% measured for Cu foils at 45°.

While Cu wire and bookend targets were also expected to deliver better spatial resolution based on MTW data, they were found to emit a higher level of high-energy photons, which wiped out the Moire fringe contrast in the images recorded on Omega EP using x-ray CCD detector since low contrast is expected to decrease signal-to-noise ratio, thus making fringe shift measurements more challenging.

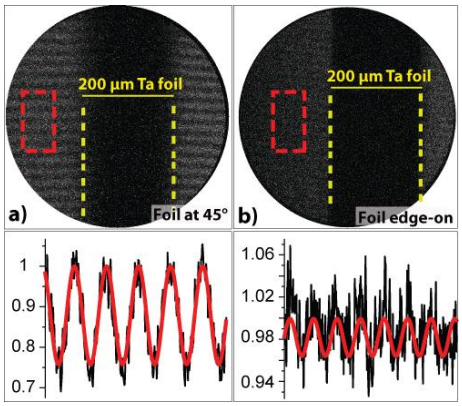

FIG. 6 Moire images of 200 µm Ta slab recorded on x-ray CCD with color enhancement. Backlighting from ~10^{17} W/cm^2 Omega EP short-pulse laser. Cu foils of 1.15×0.8mm^2×125 µm irradiated at: a) 45° and b) normal laser incidence. Normalized intensity profiles shown. Moire image color contrast enhanced to better showcase fringe shift.

The ablation front of a 3.0 x 3.0 mm^2 x 125 µm CH foil irradiated by a 160 J, 1 ns laser pulse with 120 µm spot size, was probed through TXD. An x-ray refraction angle map was retrieved, for the first time, from the Moire image recorded. Figure 7a shows a highly dense ablation front close to the foil (left side), above the TXD detection limit given by critical density (10^{25} cm^{-3}). While Moire fringe contrast was lower than expected, phase-retrieval was performed by tracking fringes individually, allowing for refraction angle mapping, as shown in Figure 7b.

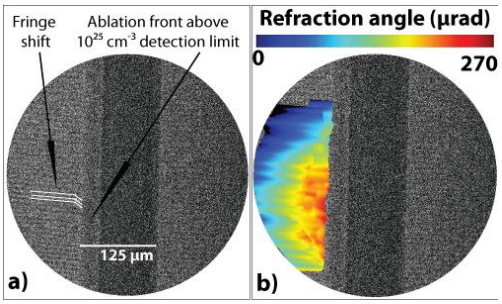

FIG. 7 a) Moire x-ray CCD image of a CH foil recoded 5 ns after main laser incidence. 8 keV backlighting at was obtained by irradiating a 1.15×0.8mm^2 ×125 µm Cu foil at 160 J, 10 ps, with 73 µm spot size at normal incidence. b) Refraction angle retrieved through TXD.

Based on these results, a new TXD variation has been designed for MTW and Omega EP. A monochromatic TXD diagnostic will use a multilayer mirror to select 8 keV emission, improving interferometer contrast by filtering out emission outside interferometer design energy. Systematic studies will optimize 8 keV emission considering spatial resolution and detector spectral response by varying target type and laser intensity (spot size and energy).

Table I below summarizes results for all laser-produced x-ray backlighters:

TABLE I. Summary of laser-produced x-ray backlighter experimental parameters. Previously unpublished data in bold.

Platform	Backlighter target (Cu)	Intensity ($\times 10^{15}$ W/cm^2)	Cu K_α (8 keV) conversion efficiency	I @8 keV ($\times 10^{12}$ W/cm^2)	Spatial resolution (μm)	Moire Fringe Contrast
MTW I	Foil 45°	50	2×10^{-4}	10	50	25% (CCD)
LULI	Wire	0.3-1.1	1.3×10^{-5}	0.004-0.014	24	7% (IP)
MTW II	Wire or Spheres	50	6×10^{-5}	3	<25	22% (CCD)
MTW III	Foil edge-on, Wire, Sphere, Bookends	8-30	$4\text{-}20 \times 10^{-5}$	0.3-6	5-10	22% (CCD) 5% (IP)
Omega EP I	Foil 45°	100-300	3×10^{-4}	30-90	>60	11-17% (CCD)
Omega EP II	Foil edge-on	200-300	2×10^{-4}	40-60	<10	3-10% (CCD)
Omega EP II	Bookends	300	7×10^{-5}	20	N/A	N/A

V. TXD FOR PULSED-POWER EXPERIMENTS

TXD diagnostics have also been implemented in the pulsed-power environment. For example, the study of the plasma density on the outside of an imploding liner in MagLIF-relevant experiments can be a straightforward and useful application. A ~350 kA, 350 ns Marx-bank pulsed-power generator, Llampudeñ[22], produced x-ray backlighting from copper x-pinch emission, allowing for electron density mapping of a low-Z object through TXD[13]. Gratings did not show any damage due to the intense magnetic field or heating induced by plasma radiation. Nevertheless, these experiments show the need of using a disposable protective filter in front of the source grating to avoid damages induced by debris from both electrodes and the plasma object.

While the x-pinch load was not properly optimized (photon fluence and source size), Moire fringe patterns with contrast up to 14% were obtained. Considering x-ray CCDs are prone to EMPs in the pulsed-power environment, Carestream D-Speed x-ray film was used as detector. It should be noted that Bio-Max equivalent x-ray film[23] is expected to deliver higher contrast and should be tested in future studies. In these experiments, the electron density of a static object was measured with <16% error[13]. Refraction angle mapping was limited by source size. These studies demonstrated TXD potential as electron density diagnostic in the pulsed-power experiment.

Follow-up experiments were carried out on GenASIS[27], a ~200 kA, 150 ns LTD generator, where a new TXD diagnostic platform was implemented. X-ray backlighting was produced by driving Cu wire[28], hybrid[29], and laser-cut[30] x-pinch loads. Emission from each load was analyzed and optimized by addressing TXD backlighter requirements[16]: spectrum, spatial and temporal resolution, emission timing, number of sources, and reproducibility.

It was found that Moire fringe contrast recorded with image plates was 0.5% for 2x25 μm Cu wire x-pinches, 1.4% for single 25 μm Cu wire hybrid x-pinches, and 7.3% with 25 μm thick Cu foil laser-cut x-pinches. This is compared to the 27% Moire fringe contrast measured with x-ray CCD using a Cu rotating anode medical x-ray tube (Fig. 8a). The much lower contrast is justified by the fact that x-ray films have higher gain at 8 keV than image plates[24–26]. Detailed analysis of these results will be published in a separate manuscript.

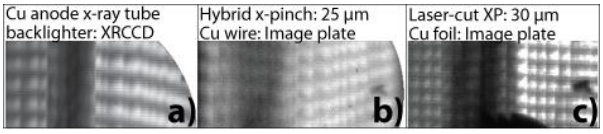

FIG. 8 Moire images of a Be sheet set at a small angle, as in Ref 13. a) Cu tube x-rays recorded with XRCCD. X-ray backlighting from: b) Hybrid x-pinch and c) Laser-cut x-pinch, recorded with image plates.

When compared to standard wire and hybrid x-pinches (Fig. 8b), laser-cut x-pinches (Fig. 8c) were found to be the optimal x-pinch configuration for TXD. Laser-cut x-pinches were found to have high reproducibility and improved spatial resolution, with source sizes measured at ≤5 μm, limited by diagnostic resolution. Their pulse duration of ~1 ns FWHM was also limited by diagnostic capabilities. Laser-cut x-pinches delivered up to 10^6 W peak power (~10^8 W/cm^2) near 8 keV, matching the optimal emission for the Talbot-Lau interferometer contrast (Fig. 3). The x-ray backlighting properties of the three x-pinch configurations can be found in Ref. 31.

The electron density of a Be sheet of 0.5×2.5×5.0 mm^3 was retrieved from Moire images. The Be sheet was set at a small angle so that edges produce a constant fringe shift while the center of the object produces no shift. Conversely, attenuation varies at the edges and is constant at the center. Following Equation 1 and considering that one fringe shift is equivalent to the system W_{eff} (199 μrads), an electron density of $4.39 \pm 1.43 \times 10^{23}$ cm^{-3} was retrieved for the Hybrid X-pinch (Fig. 8b), representing 11.1% underestimation of the tabulated value. Laser-cut x-pinches (Fig. 8c) delivered an electron density of $5.13 \pm 2.48 \times 10^{23}$ cm^{-3}, representing an overestimation of the tabulated value by 3.8%, which is well within the measurement uncertainty.

Plasma loads were imaged through TXD for the first-time using laser-cut x-pinch backlighting[31]. These results will be presented and discussed thoroughly elsewhere. Experimental images matched XWFP simulations[32], demonstrating TXD can be a powerful x-ray refraction-based diagnostic for dense Z-pinch loads.

VI. SUMMARY

The development of TXD diagnostics for HEDP experiments has been presented. Grating survival and Moiré

fringe formation have been demonstrated in the high-intensity laser and pulsed-power environments. Refraction angle mapping and electron density retrieval was achieved with Cu backlighter targets. Thin foils, wires, and spheres were irradiated by 10-150 J, 8-30 ps laser pulses to produce K_α emission in the MTW, LULI2000, and Omega EP laser systems. Additionally, Llampudkeñ (~350 kA, 350 ns) and GenASIS (~200 kA, 150 ns) pulsed-power generators used Cu wire x-pinch loads. GenASIS was also used to drive novel configurations: hybrid and laser-cut x-pinches. X-ray backlighting was provided by Cu K_α emission (8 keV). Electron density profiles were retrieved achieving 4-11% accuracy when compared to tabulated values. The first x-ray images of plasma objects recorded through TXD were obtained. The ablation front of a laser-irradiated CH foil was imaged through TXD for the first time on OMEGA EP for densities $>10^{23}$ cm^{-3}, and a refraction angle map was obtained from post-processing. X-ray backlighting for TXD was optimized considering targets and detectors. It was shown that target type can improve spatial resolution, while detector choice can optimize Moire fringe contrast, thus achieving accurate plasma characterization through TXD.

VI. ACKNOWLEDGMENTS

Work supported by: NNSA: NLUF DE-NA0002955 and HEDLP DE-NA0003882 and DE-NA0003842. DoE Office of Science FES: DE-SC0020005 LaserNetUS (Omega Laser Facility). Fondecyt No. 1171412. The authors thank LLE science and engineering staff for their support throughout the years as well as students and professors from Pontificia Universidad Catolica de Chile, U. of Michigan, École Polytechnique, and Johns Hopkins University.

VI. DATA AVAILABILITY

Data available from the authors upon request.

VII. REFERENCES

1. Stutman, D. & Finkenthal, M. Talbot-Lau x-ray interferometry for high energy density plasma diagnostic. *Rev. Sci. Instrum.* **82**, 113508 (2011).
2. Valdivia, M. P., Stutman, D. & Finkenthal, M. Moire deflectometry using the Talbot-Lau interferometer as refraction diagnostic for High Energy Density plasmas at energies below 10 keV. *Rev. Sci. Instrum.* **85**, 073702 (2014).
3. Mayo, S. C., Stevenson, A. W. & Wilkins, S. W. In-Line Phase-Contrast X-ray Imaging and Tomography for Materials Science. *Materials (Basel).* **5**, 937–965 (2012).
4. Pfeiffer, F., Weitkamp, T., Bunk, O. & David, C. Phase retrieval and differential phase-contrast imaging with low-brilliance X-ray sources. *Nat. Phys.* **2**, 258–261 (2006).
5. Valdivia, M. P., Stutman, D. & Finkenthal, M. Talbot-Lau based Moiré deflectometry with non-coherent sources as potential High Energy Density plasma diagnostic. *J. Appl. Phys.* **114**, 163302 (2013).
6. Valdivia, M., Stutman, D. & Finkenthal, M. Talbot-Lau x-ray density diagnostic for High Energy Density plasmas. *2015 IEEE 26th Symp. Fusion Eng.* 1–5 (2015) doi:10.1109/SOFE.2015.7482292.
7. Jahns, J. & Lohmann, A. W. The Lau effect (a diffraction experiment with incoherent illumination). *Opt. Commun.* **28**, 263–267 (1979).
8. Morimoto, N., Fujino, S., Ohshima, K., Harada, J. & Hosoi, T. X-ray phase contrast imaging by compact Talbot – Lau interferometer. **39**, 4297–4300 (2014).
9. Liu, L. Partially coherent diffraction effect between Lau and Talbot effects. *J. Opt. Soc. Am. A* **5**, 1709 (1988).
10. Case, W. B., Tomandl, M., Deachapunya, S. & Arndt, M. Realization of optical carpets in the Talbot and Talbot-Lau configurations. *Opt. Express* **17**, 20966 (2009).
11. Stutman, D., Finkenthal, M. & Moldovan, N. Development of optics for x-ray phase-contrast imaging of high energy density plasmas. *Rev. Sci. Instrum.* **81**, 10E504 (2010).
12. Bouffetier, V. *et al.* Proof-of-concept Talbot – Lau x-ray interferometry laser-driven K-alpha source. *Appl. Opt.* **59**, 8380–8387 (2020).
13. Vescovi, M., Valdivia, M. P., Veloso, F., Stutman, D. & Favre, M. Implementation of Talbot–Lau x-ray deflectometry in the pulsed power environment using a copper X-pinch backlighter. *J. Appl. Phys.* **127**, 203301 (2020).
14. Donath, T. *et al.* Inverse geometry for grating-based x-ray phase-contrast imaging. *J. Appl. Phys.* **106**, 2049–2064 (2009).
15. Valdivia, M. P. *et al.* An x-ray backlit Talbot-Lau deflectometer for high-energy-density electron density diagnostics. *Rev. Sci. Instrum.* **87**, 023505 (2016).
16. Valdivia, M. P. *et al.* X-ray backlighter requirements for refraction-based electron density diagnostics through Talbot-Lau deflectometry. *Rev. Sci. Instrum.* **89**, 138–145 (2018).
17. Valdivia, M. P. *et al.* Implementation of a Talbot – Lau x-ray deflectometer diagnostic platform for the OMEGA EP laser Implementation of a Talbot – Lau x-ray deflectometer diagnostic platform for the OMEGA EP laser. *Rev. Sci. Instrum.* **91**, 023511 (2020).
18. Rigon, G. *et al.* Rayleigh-Taylor Instability experiments on the LULI2000 laser Facility in scaled conditions for Supernovae Remnants of a few hundred years. *Phys. Rev. E* **100**, 021201 (2019).
19. Theobald, W. *et al.* High-intensity laser-plasma interaction with wedge-shaped-cavity targets. *Phys. Plasmas* **17**, 1–7 (2010).
20. Nilson, P. M. *et al.* Scaling Hot-Electron Generation to High-Power , Kilojoule-Class Laser-Solid Interactions. *Phys. Rev. Lett.* **105**, 235001 (2010).
21. Nilson, P. M. *et al.* Time-resolved Ka spectroscopy measurements of hot-electron equilibration dynamics in thin-foil solid targets: collisional and collective effects. *J. Phys. B At. Mol. Opt. Phys.* **48**, 224001 (2015).
22. Chuaqui, H., Wyndham, E., Friedli, C. & Favre, M. LLAMPÜDKEÑ: A high-current, low-impedance pulser employing an auxiliary exponential transmission line. *Laser Part. Beams* **15**, 241 (1997).
23. Marshall, F. J., Knauer, J. P., Anderson, D. & Schmitt, B. L. Absolute calibration of Kodak Biomax-MS film response to x rays in the 1 . 5- to 8-keV energy range. *Rev. Sci. Instrum.* **77**, 10F308 (2006).
24. Lanier, N. E., Cowan, J. S. & Workman, J. Characterization and cross calibration of Agfa D4 , D7 , and D8 and Kodak SR45 x-ray films against direct exposure film at 4 . 0 – 5 . 5 keV. *Rev. Sci. Instrum.* **77**, 043504 (2006).
25. Haugh, M. J., Lee, J., Romano, E. & Schneider, M. Calibrating image plate sensitivity in the 700 to 5000 eV spectral energy range. *Target Diagnostics Phys. Eng. Inert. Confin. Fusion II* **8850**, 885007 (2013).
26. Chen, H. *et al.* Absolute calibration of image plates for electrons at energy between 100 keV and 4 MeV. *Rev. Sci. Instrum.* **79**, 3–6 (2008).
27. Bott, S. *et al.* 250 kA compact linear transformer driver for wire array z-pinch loads. *Phys. Rev. Spec. Top. - Accel. Beams* **14**, 1–8 (2011).
28. Kalantar, D. H. & Hammer, D. A. The x-pinch as a point source of x rays for backlighting. *Rev. Sci. Instrum.* **66**, 779–781 (1995).
29. Shelkovenko, T. A. *et al.* Hybrid X-pinch with conical electrodes. *Phys. Plasmas* **17**, 112707 (2010).
30. Collins, G. W. *et al.* Investigation into the dynamics of laser-cut foil X-pinches and their potential use for high repetition rate operation. *Appl. Phys. Lett.* **105**, 024101 (2014).
31. Collins IV, G. W. *et al.* Direct comparison of wire, foil, and hybrid X-pinches on a 200 kA, 150 ns current driver. *J. Appl. Phys.* **129**,.
32. Weitkamp, T. XWFP: an x-ray wavefront propagation software package for the IDL computer language. *Adv. Comput. Methods X-Ray Neutron Opt.* **5536**, 181–189 (2004).

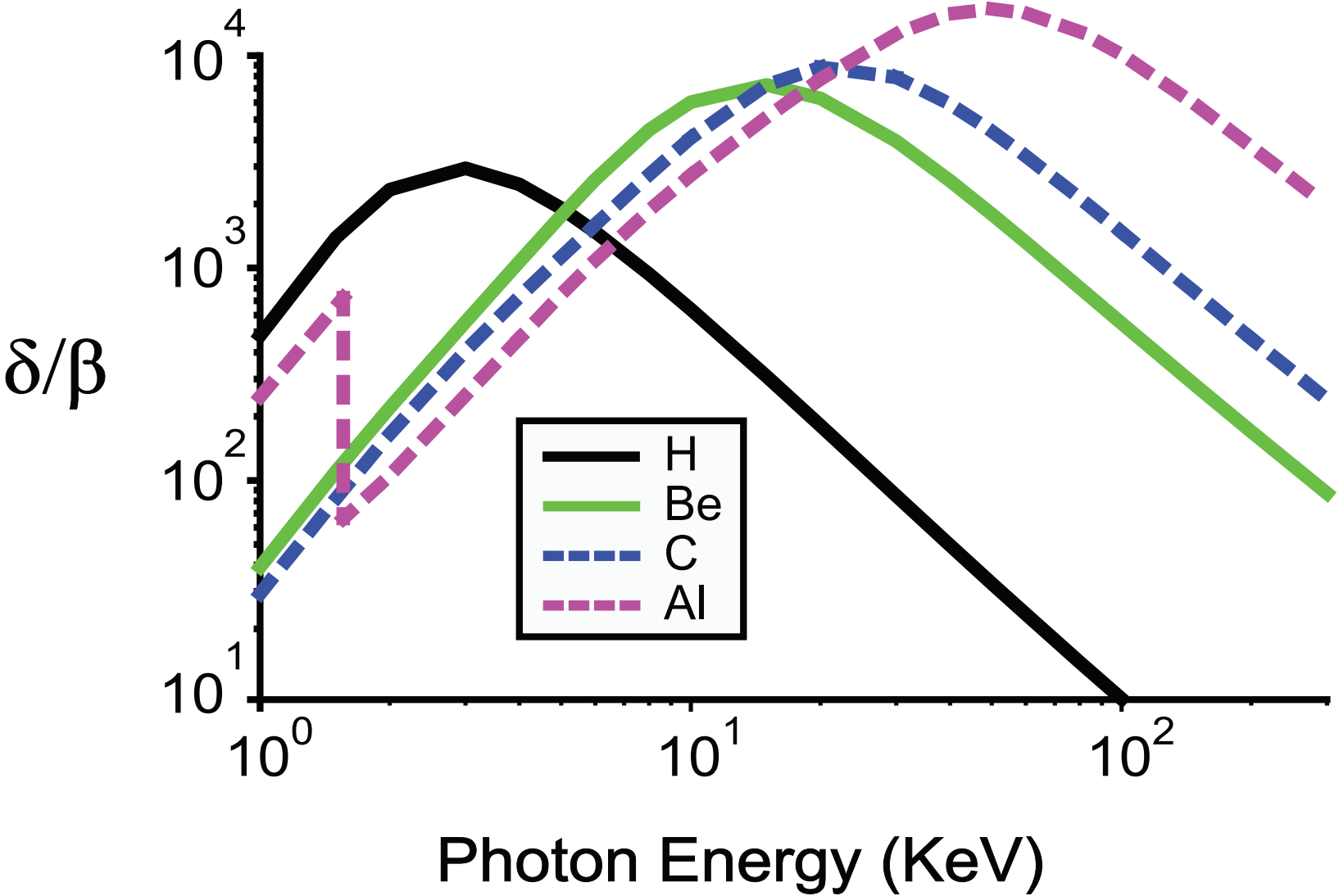
δ/β
10^4
10^3
10^2
10^1
10^0
10^1
10^2
H
Be
C
Al
Photon Energy (KeV)

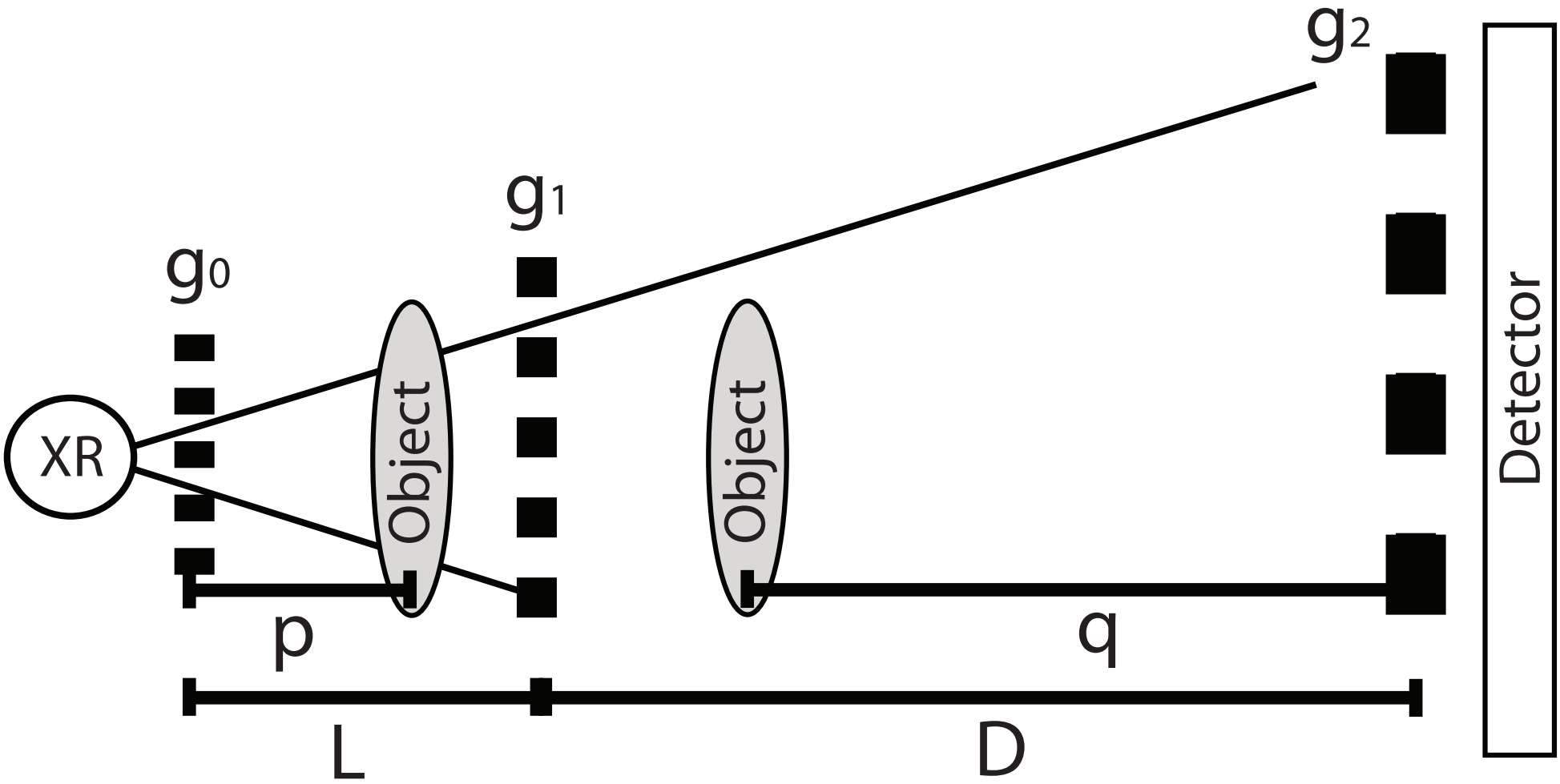
g2
g1
g0
XR
Object
Object
Detector
p
q
L
D

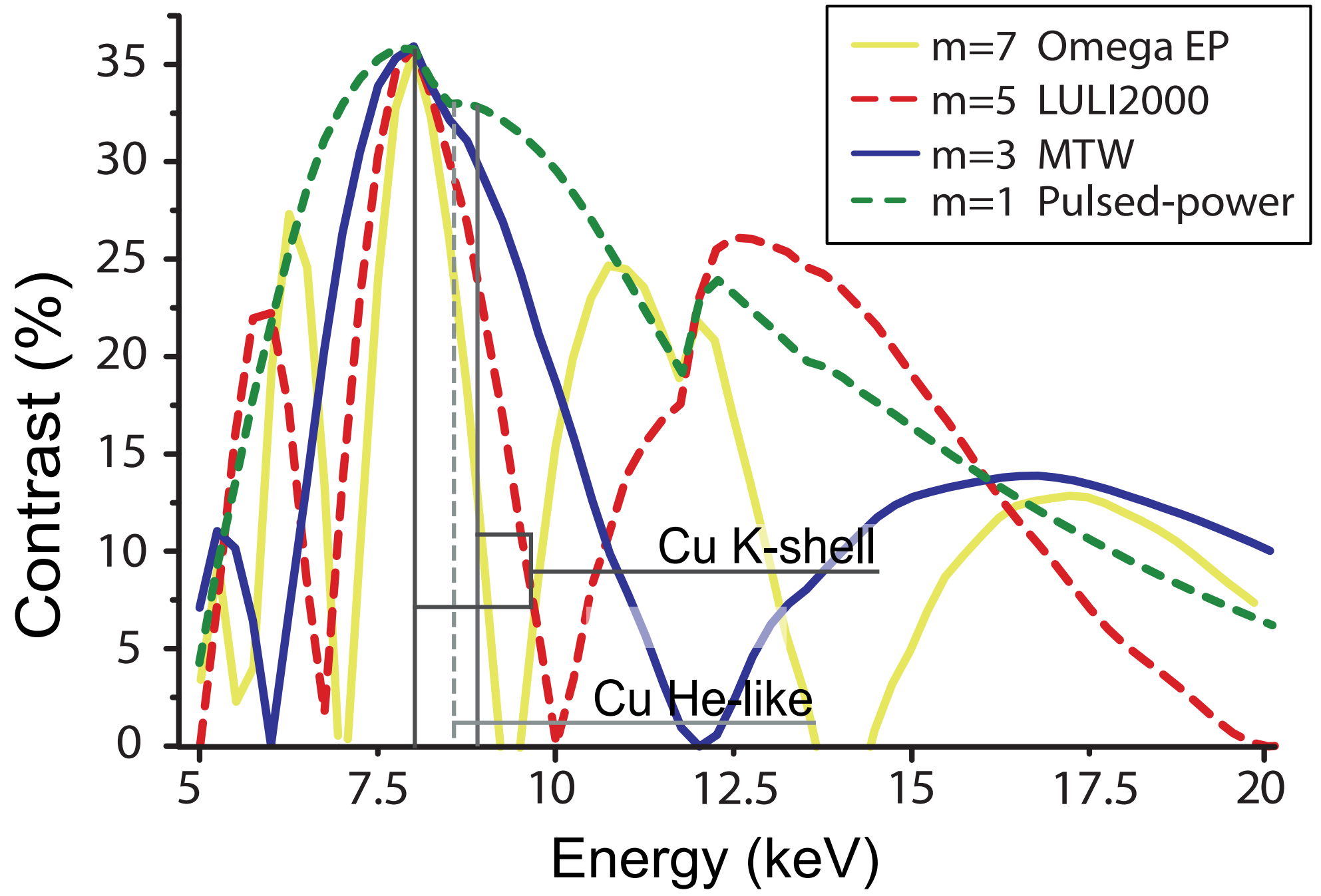
m=7 Omega EP
m=5 LULI2000
m=3 MTW
m=1 Pulsed-power
Cu K-shell
Cu He-like
Contrast (%)
Energy (keV)
0
5
10
15
20
25
30
35
5
7.5
10
12.5
15
17.5
20

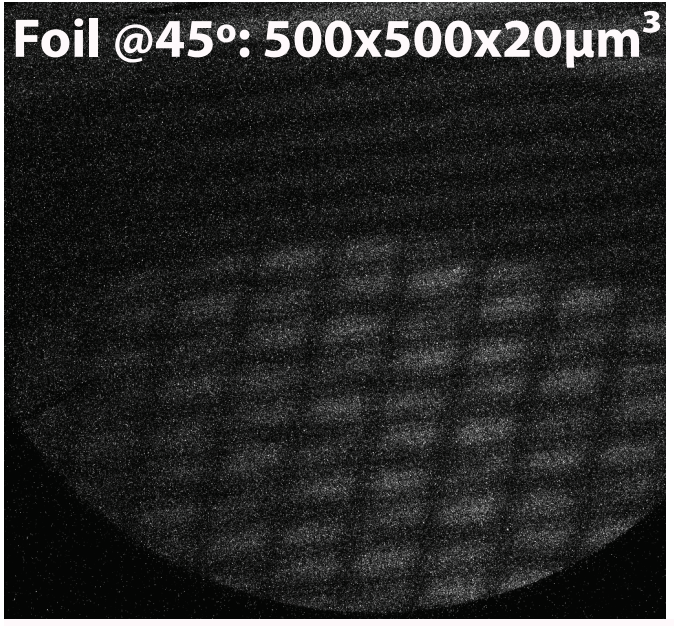
Foil @45°: 500x500x20μm³

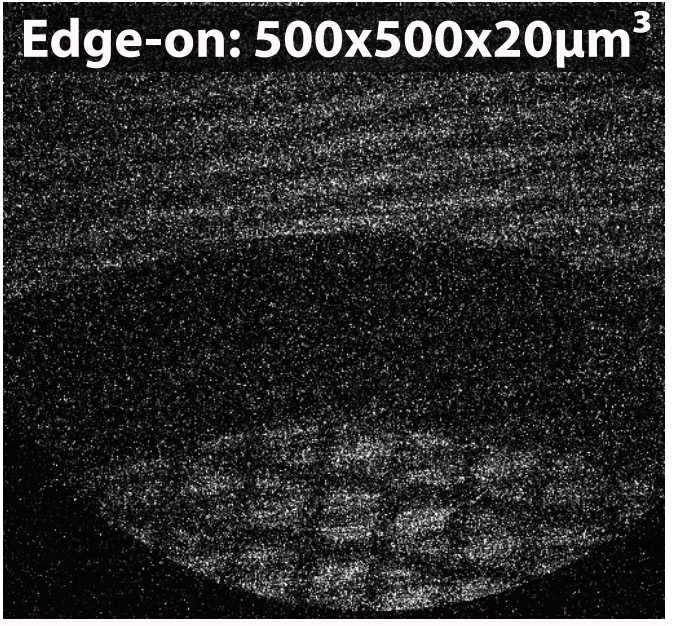
Edge-on: 500x500x20μm³

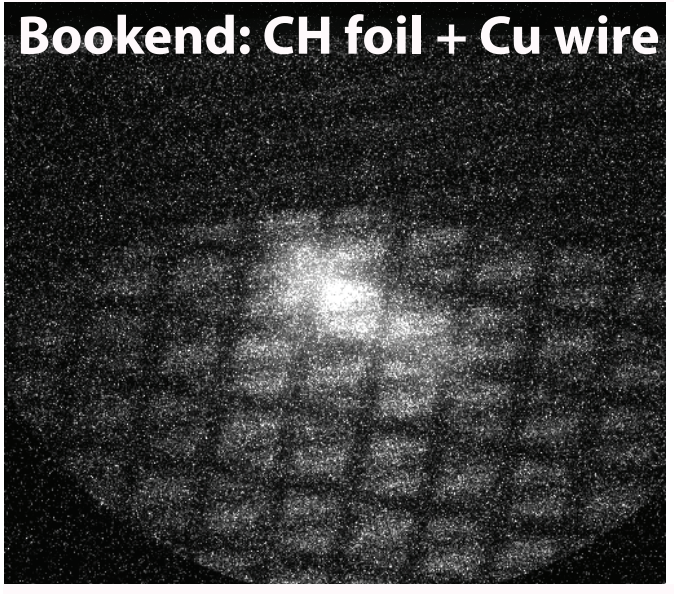
Bookend: CH foil + Cu wire

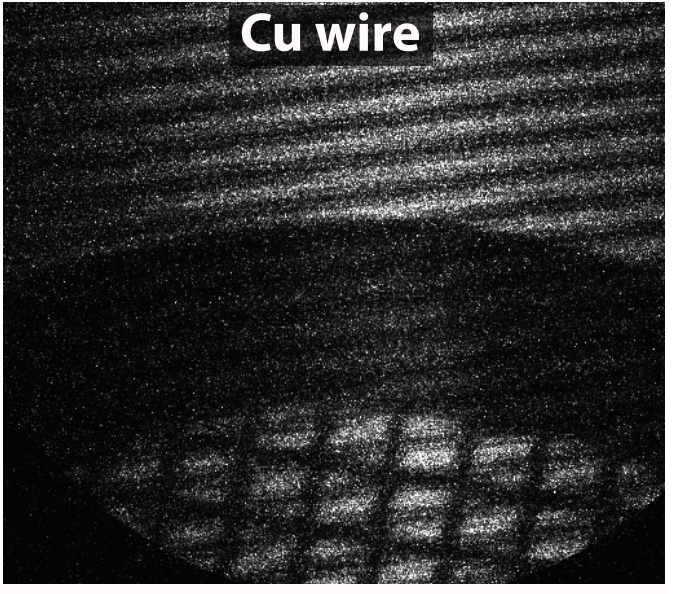
Cu wire

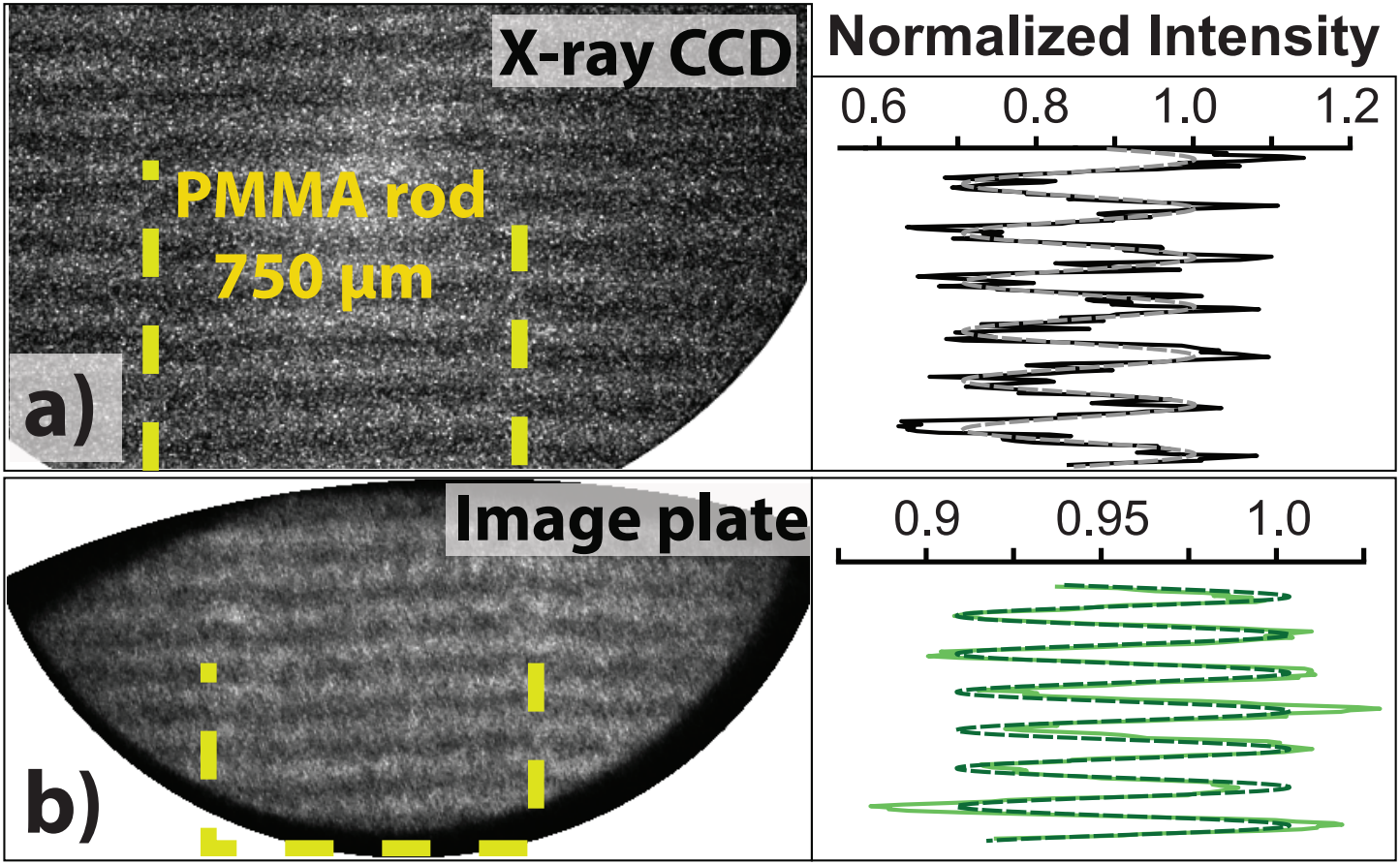
X-ray CCD
PMMA rod
750 µm
a)
Normalized Intensity
0.6
0.8
1.0
1.2
Image plate
b)
0.9
0.95
1.0

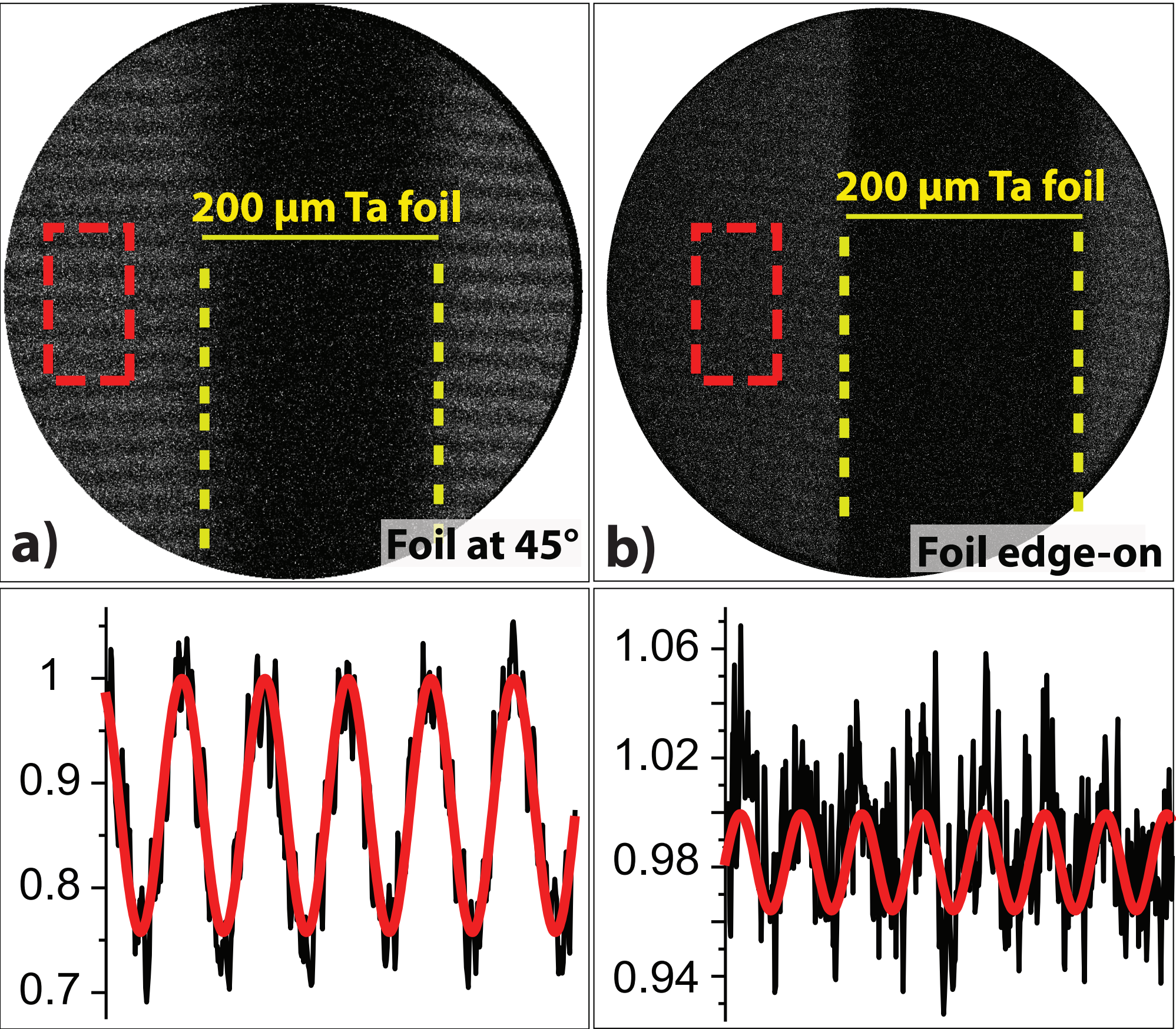
200 µm Ta foil
a)
Foil at 45°
200 µm Ta foil
b)
Foil edge-on
1
0.9
0.8
0.7
1.06
1.02
0.98
0.94

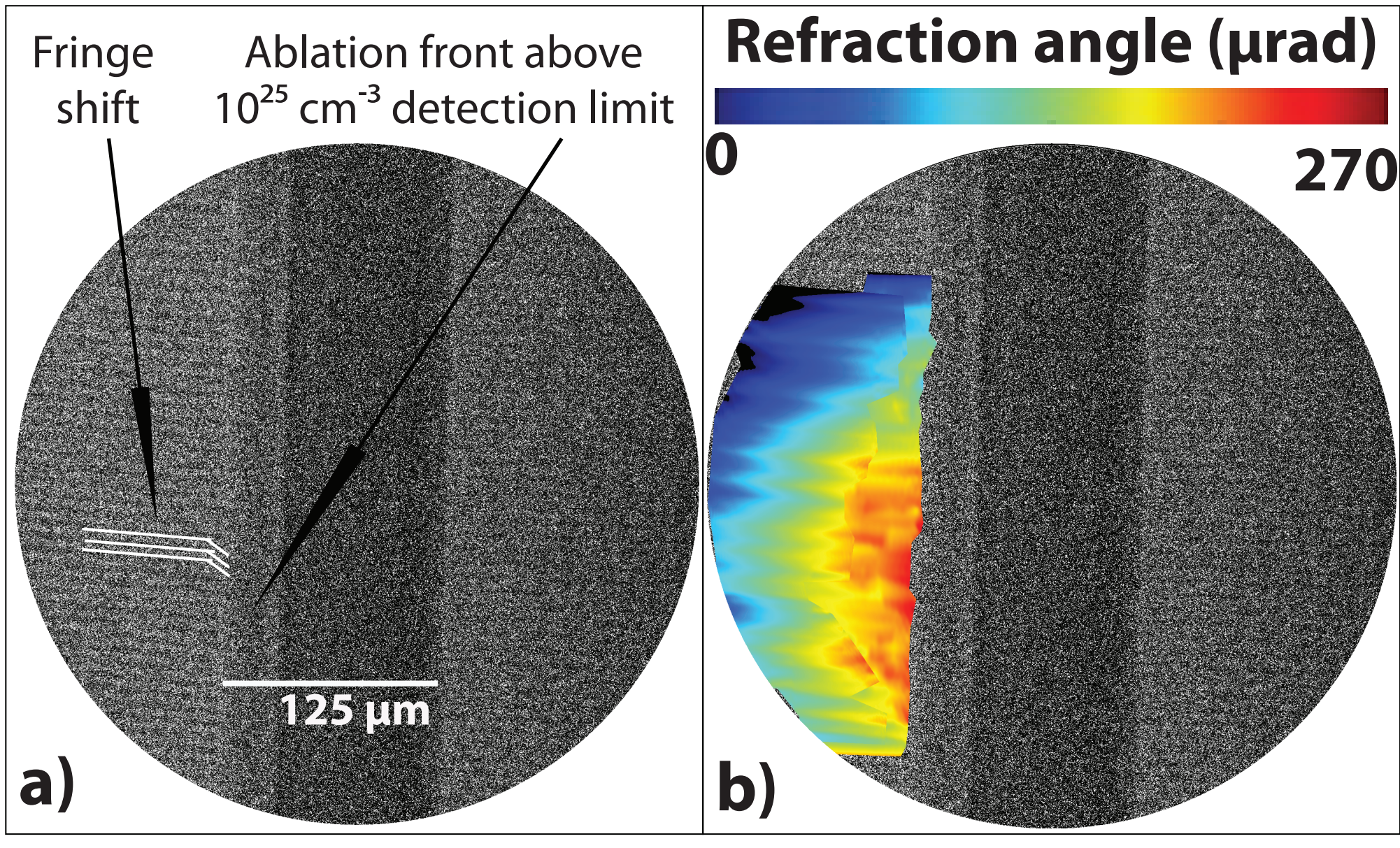
Fringe shift
Ablation front above 10^{25} cm^{-3} detection limit
125 µm
a)
Refraction angle (µrad)
0
270
b)

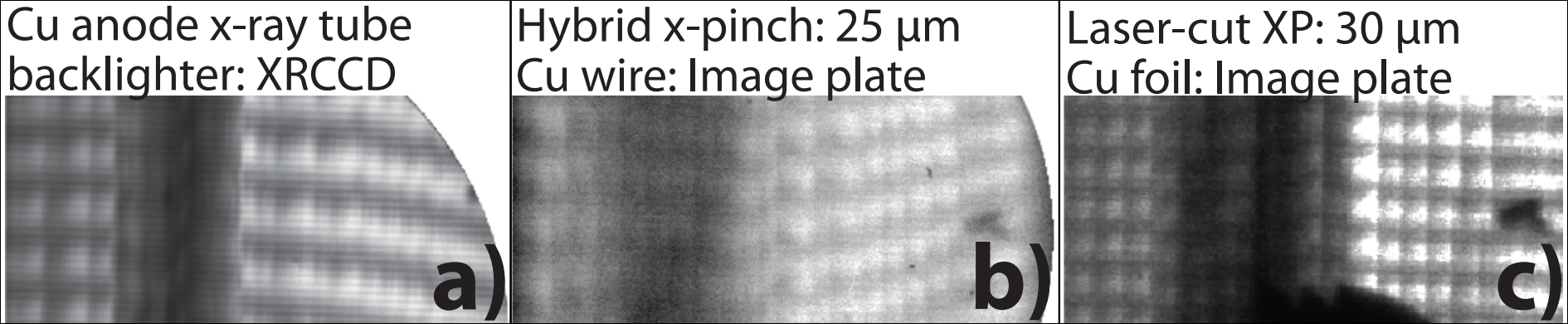
Cu anode x-ray tube
backlighter: XRCCD
a)
Hybrid x-pinch: 25 μm
Cu wire: Image plate
b)
Laser-cut XP: 30 μm
Cu foil: Image plate
c)